RSC Advances

PAPER

View Article Online
View Journal | View Issue

Check for updates

Cite this: *RSC Adv.*, 2023, **13**, 4138

First-principles calculations to investigate physical properties of orthorhombic perovskite YBO_3 (B = Ti & Fe) for high energy applications

Ahmed Azzouz Rached, *[a] Ismail Ouadha,[a] Mudasser Husain,[b] Habib Rached, [ac] Hamza Rekab-Djabri,[de] Ali Bentouaf, [fg] Tariq Hadji,[c] Nourreddine Sfina,[hi] Hind Albawali,[j] Vineet Tirth, [kl] Mohammed A. Amin[m] and Nasir Rahman *[b]

Orthorhombic oxide perovskite compounds are very promising materials for the applications of optoelectronics and thermal barrier coating. This work represents a numerical simulation of YBO_3 compounds through the first-principles *ab initio* approach. The electronic and magnetic properties are investigated employing the general gradient approximation (GGA) coupled to the integration of the Hubbard U-term which is the GGA + U. The Ti and Fe-based YBO_3 perovskite compounds are found to be actively promising within the ferromagnetic configuration and their lattice parameters are consistent with the previous studies. The calculations of formation energy signify that the compounds YBO_3 are stable thermodynamically. The electronic properties are computed and evaluated by the band structure and density of states for both compounds and the results depict that these materials are ferromagnetic half-metallic. Mechanically these compounds are stable, ductile, anisotropic, and hard to scratch. The thermal properties are evaluated for YBO_3 (B = Ti and Fe) compounds up to a temperature range of 2000 K. This work can open new opportunities for further exploration in this field.

Received 4th December 2022
Accepted 23rd January 2023

DOI: 10.1039/d2ra07727b

rsc.li/rsc-advances

Open Access Article. Published on 31 January 2023. Downloaded on 12/12/2025 10:45:39 AM.
This article is licensed under a Creative Commons Attribution-NonCommercial 3.0 Unported Licence.

1. Introduction

Nowadays, the scientific community is searching for ductile, stiff, non-corrosive, and strong materials at higher temperatures and pressure regarding their use in modern technological applications. These industrial and technological applications include the medical, automobile, aerospace, defense, sensors, nuclear industry, portable electronic devices, electrical contacts, protective coatings, high-temperature structural applications, and thermal barrier coatings.[1–4] Recently, ABO_3 perovskite oxide compounds have achieved greater attention owing to an appropriate grouping of thermo-mechanical properties at high temperatures and pressure.[5–7] However, the paucity of research examining the mechanical and thermal properties at high pressure of perovskite compounds hampers endeavors toward the recognition of improved high-energy applications. Understanding the property conveyance in the perovskite compounds family, as well as the creation of a suitable screening mechanism, are critical for accelerating the design and disclosure of perovskite-based high-energy applications.[6–8]

The properties and applications of the perovskite have been growing in interest in the scientific community over the past years.[9–11] Consequently, some exceptional hydraulic stress perovskite, it has proven to be an alternative to chemical pressure. In this continuation, very recently, arnab majumdar *et al.* investegated four novel perovskites $AZrS_3$ where A = Mg, Ca, Sr and Ba. Upon being compressed, the direct band gaps decrease

[a]*Magnetic Materials Laboratory, Faculty of Exact Sciences, Djillali Liabes University of Sidi Bel-Abbes, Algeria. E-mail: a.azzouzrached@univ-chlef.dz*
[b]*Department of Physics, University of Lakki Marwat, 28420, Lakki Marwat, Khyber Pukhtunkhwa, Pakistan. E-mail: nasir@ulm.edu.pk*
[c]*Department of Physics, Faculty of Exact Sciences and Informatics, Hassiba Benbouali University of Chlef, Algeria*
[d]*Laboratory of Micro and Nanophysics (LaMiN), National Polytechnic School Oran, ENPO-MA, BP 1523, El M'Naouer, 31000, Oran, Algeria*
[e]*Faculty of Nature and Life Sciences and Earth Sciences, AkliMohand-Oulhadj University, 10000, Bouira, Algeria*
[f]*Laboratory of Physical Chemistry of Advanced Materials, Djillali Liabés University of Sidi Bel-Abbès, 22000, Sidi Bel-Abbès, Algeria*
[g]*Faculty of Technology, Dr Moulay, Tahar University of Saida, 20000, Saida, Algeria*
[h]*College of Sciences and Arts in Mahayel Asir, Department of Physics, King Khalid University, Abha, Saudi Arabia*
[i]*Laboratoire de la Matière Condensée et des Nanosciences (LMCN), Département de Physique, Faculté des Sciences de Monastir, Université de Monastir, Avenue de l'Environnement, 5019 Monastir, Tunisia*
[j]*Department of Physics, College of Sciences, Princess Nourah bint Abdulrahman University (PNU), P.O. Box 84428, Riyadh 11671, Saudi Arabia*
[k]*Mechanical Engineering Department, College of Engineering, King Khalid University, Abha 61421, Kingdom of Saudi Arabia*
[l]*Research Center for Advanced Materials Science (RCAMS), King Khalid University, Guraiger, P.O. Box No. 9004, Abha 61413, Asir, Kingdom of Saudi Arabia*
[m]*Department of Chemistry, College of Science, Taif University, P.O. Box 11099, Taif 21944, Saudi Arabia*

© 2023 The Author(s). Published by the Royal Society of Chemistry

Open Access Article. Published on 31 January 2023. Downloaded on 12/12/2025 10:45:39 AM.
This article is licensed under a Creative Commons Attribution-NonCommercial 3.0 Unported Licence.

to desired values which can render this class of zirconium based chalcogenide perovskites to be used in tandem solar cells. They found that when pressure is applied, the direct band gaps decrease to desired values which can render this class of zirconium based chalcogenide perovskites to be used in tandem solar cells.[12] And the same search group has explored on the physical properties and defect processes of cubic and tetragonal $BaSrN_3$ at 100 GPa using an *ab initio* structure search method, and informed that these results predicted to be the design of cleaner and environmentally friendly high energy density materials.[13] The ternary oxides perovskites compounds possess a large family of atomically layered materials having the same crystalline structure and the general chemical formula of ABX_3 (A is a rare earth or alkaline or alkaline earth materials, B is a transition metal, and X is mostly oxygen).[14,15] Due to various widespread uses in numerous technologies, the quest for novel materials for specific purposes is getting popular. Machine learning approaches and *ab-initio* computations employing DFT allowed for the screening of enormous sets of materials. Several systems comprising oxides perovskites are being studied, and the results have been published in recent years using machine learning and DFT.[16,17] Wakil Hasan *et al.*[18] recently reported indium-based oxides perovskites $TlBO_3$ (B = Cr, Mn) employing DFT within WIEN2K and have shown that lower values of thermal conductivity and high values of Debye temperature in the $TlBO_3$ (B = Cr, Mn) compounds may be applied as a promising material for thermoelectric and unfriendly environments. Furthermore, the ground-state physical properties of $Pb(Mg_{1/3}Nb_{2/3})O_3$ compounds are predicted to be the most tolerant material for thermal barrier coating.[19] Numerous studies reported the halides and oxides perovskites and MAX phase which possesses the physical, mechanical, and chemical properties because of the potential applications in various fields,[4–7,20–22] and it is observed that our investigated results, show consistency with the available results in the literature. So, this class of materials perovskite oxides promising applications for enlightening properties for various technologically equipped societies.

2. Computational method

The investigated data presented in this work is obtained by employing all electrons FP-LAPW (full-potential linearized augmented plane wave) technique within the WIEN2K code.[23–25] This method is grounded on DFT (density functional theory) in which PBE-GGA (Perdew–Burke–Ernzerhof generalized gradient approximations),[26,27] is employed for magnetic and electronic properties. The GGA + U approximation is utilized here[28–31] for the investigations of interesting physical properties. The $U_{eff} = U - J$ (effective on-site Coulomb exchange correlations) is adopted, whereas "*U*" is the Coulomb *U* parameter and "*J*" represent an exchange parameter. Since U_{eff} is known for transition metal elements and its value is from 2 and 6 eV[32,33] and in our work, the value of U_{eff} is selected to be 2 eV for transition metal atoms selected and reported.[34–36] The parameter muffin-tin (MT) radii picked is 2.1, 1.92, and 1.74 Bohr for Y, B = (Ti and Fe) and "O" atoms respectively. The $l_{max} = 10$ is the maximum value for charge density inside the atomic spheres selected and the charge density Fourier expansion of the magnitude of the largest vector $G_{max} = 14$ is chosen. For better convergence, the convergence has been reached to the energy and the charge are less than 0.00001 Ry and 0.0001 e/a.u.^{3}, respectively. And an 11 × 11 × 4 Monkhorst–Pack *k*-point grid is used for integration over the Brillouin zone (BZ).

3. Results and discussion

In this part, the investigated results of the various physical properties of the orthorhombic oxides perovskite YBO_3 (B = Ti & Fe) is presented and discussed in detail.

3.1. Structural properties

The structure of perovskite oxide YBO_3 is orthorhombic having the space group of *Pbnm* (No. 62) as depicted in Fig. 1a. The YBO_3 type structure consists of Y, B, O1 and O2 atoms that occur at positions 4c, 4b, 4c and 8d respectively. To investigate the

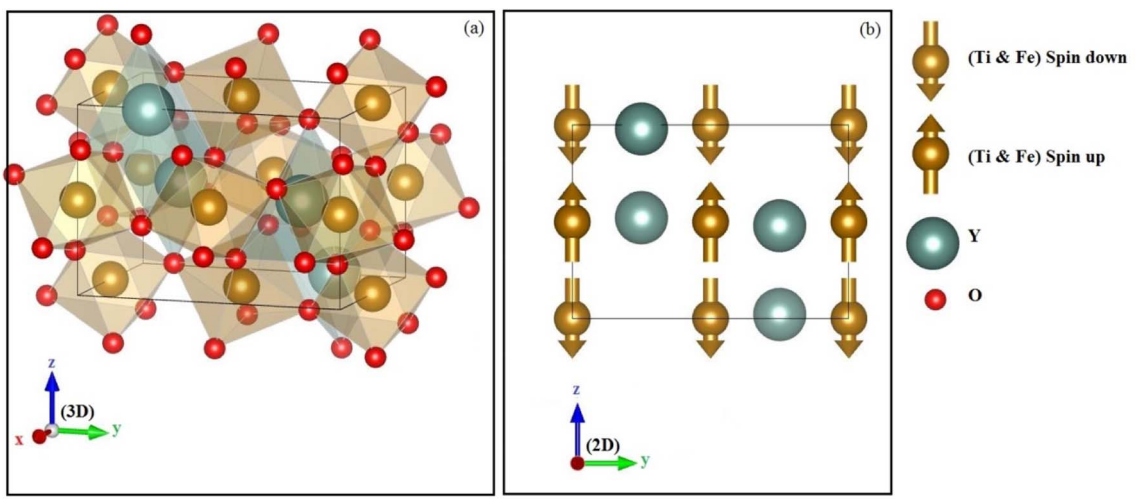

Fig. 1 The (a) crystal structure and (b) antiferromagnetic configuration within orthorhombic oxides perovskite YBO_3 (B = Ti, Fe).

Open Access Article. Published on 31 January 2023. Downloaded on 12/12/2025 10:45:39 AM. This article is licensed under a Creative Commons Attribution-NonCommercial 3.0 Unported Licence.

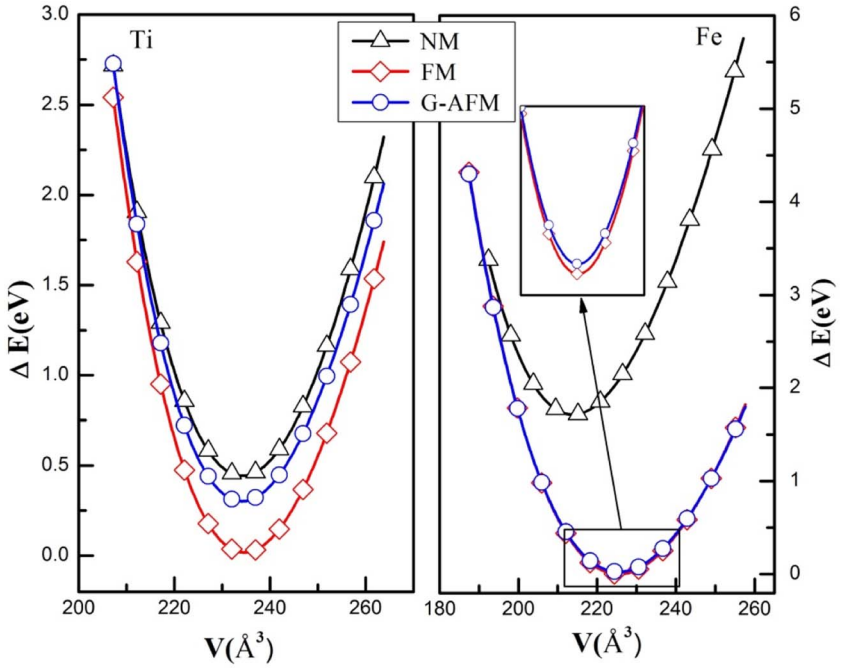

Fig. 2 The energy *versus* volume fit for NM, FM, and G-AFM scheme of YBO_3 (B = Ti, Fe) compounds.

equilibrium crystal structural parameters of the two selected compounds for different magnetic configurations, we have considered spin orientation for antiferromagnetic (AFM) as shown in Fig. 1b. The total energy *vs.* the volume of the two compounds for different magnetic configurations is computed and the results are fitted using Murnaghan's EOS (equation of states) and presented in Fig. 2.

The FM (ferromagnetic) state has the lowest energy than other states for both compounds. Therefore, one can assert that YBO_3 (B = Ti, Fe) compounds are stable in the FM phase. The calculated structural parameters and other theoretical results are listed in Table 1. It is noted here that our computed results settle well with existing experimental and theoretical data. These parameters are very important for calculating other properties like ductility, hardness, thermal and magnetic properties, *etc.*

To examine the material ability and stability, we estimated the formation energy (E_f) of the YBO_3 orthorhombic perovskite using the following expression.[39–43]

$$\Delta H_f(YBO_3) = E_{tot}(YBO_3) - (aE(Y) + bE(B) + cE(O)); \text{ B} = \text{Ti, Fe} \quad (1)$$

Here, a, b and c represent the number of atoms of "Y", (Ti/Fe), and O, respectively inside the unit cell, the formation energy is represented by $\Delta H_f(YBO_3)$ for YBO_3 (B = Ti and Fe), the total energy per unit cell is depicted by $E_{tot}(YBO_3)$ for the bulk YBO_3 compounds and E(Y), E(B) and E(O) are the total energies of Y, Ti/Fe, and O, respectively within the crystalline structure. The negative formation energies are obtained for both compounds, indicating the stability against disintegration into their constituent elements. The present value of formation energy for

Table 1 Computed lattice parameters (a, b, and c), volume (V), bulk modulus (B), and total energy of YBO_3 (B = Ti, Fe) compounds

Compounds	Phase	Cell parameters (Å)			V (Å^3)	B (GPa)	Total energy (Ry)
		a	b	c			
$YTiO_3$	NM	5.7030	7.7050	5.3398	234.6668	194.0980	−35725.356614
	FM	5.7107	7.6973	5.3376	234.6491	195.3640	−35725.38919
	G-AFM	5.7070	7.6919	5.3342	234.1637	194.2559	−35725.367055
$YFeO_3$	NM	5.5009	7.4103	5.2463	213.8634	205.6982	−39075.958642
	FM	5.6356	7.5663	5.2888	225.5225	159.5047	−39076.084552
	G-AFM	5.6348	7.5648	5.2877	225.3998	156.0757	−39076.084531
		5.5907[a]	7.6082[a]	5.2849[a]	224.79[a]	—	—
		5.5961[b]	7.6098[b]	5.2855[b]	225.08[b]	—	—

[a] Ref. 37. [b] Ref. 38.

© 2023 The Author(s). Published by the Royal Society of Chemistry

Open Access Article. Published on 31 January 2023. Downloaded on 12/12/2025 10:45:39 AM.
This article is licensed under a Creative Commons Attribution-NonCommercial 3.0 Unported Licence.

$YTiO_3$ and $YFeO_3$ is −0.580 eV per atom, and −0.521 eV per atom, respectively.

3.2. Phonon dispersion

To confirm the thermodynamically stabilities of the compounds, we evaluate the dynamic stability by calculating the phonon band structure using the finite displacement method implemented in the WIEN2K package within the frequency range from 0 THz up to 30 THz, as depicted in Fig. 3. It can be seen from Fig. 3 that the phonon dispersion curves for both materials are positive and there are no negative values of dispersion curves (imaginary phonon frequencies). The positive dispersion curves confirm the phonon dynamical stability of both compounds.

3.3. Electronic structure and magnetic moment

The electronic structure (ES) can support to elucidate us information to understand the behavior of electrons within materials, it is used in electrical industries, electronics, and microelectronics. The electronic structure investigated for the YBO_3 compounds is considered in the stable phase by investigating the electronic band structure (EBS) and density of states (DOS) for the spins up and down within the framework of GGA + U using $U = 2$ eV in these investigations for transition metals-3d states. Fig. 4, depicts the spin-resolved EBS and TDOS of our compounds. The computation shows that both the two materials in the spin-up channel cross at the E_F (Fermi level), whereas those in the spin-down channel have semiconductor characteristics, indicating that the compounds of interest exhibit a ferromagnetic half-metallic (FM-HM) nature. The TDOS findings demonstrated full agreement with EBS.

To further understand the nature of the EBS, we estimated the PDOS for both channels, which are shown in Fig. 5. TDOS along with PDOS are plotted within the −8 eV to 7 eV energy range, in which the contribution of the total density of the constituent element and the partial contribution from the state of the concerning element is shown and described. The elemental and states contribution to the valence band and conduction band are depicted, and it is very clear that the major contribution to the electronic states within the valence band is occur from the In-p state, (Fe, Ti)-d state, and O-p state. In discussing the conduction band from 0 eV to 7 eV energy level, we see that the dominant part possesses the (Fe, Ti)-d state with little contribution from the "Y" element.

In this paragraph, we highlight the magnetic properties, because these properties are related to numerous electronic applications such as radiation shielding, sensors, and induction heating. The total and atomic magnetic moments of YBO_3 (B = Ti, Fe) compounds are calculated and summarized in Table 2. It is worth noting that the overall magnetic moments of $YTiO_3$ and $YFeO_3$ compounds are carried by Ti/Fe atoms which give 4 μ_B and 12 μ_B in total, respectively.

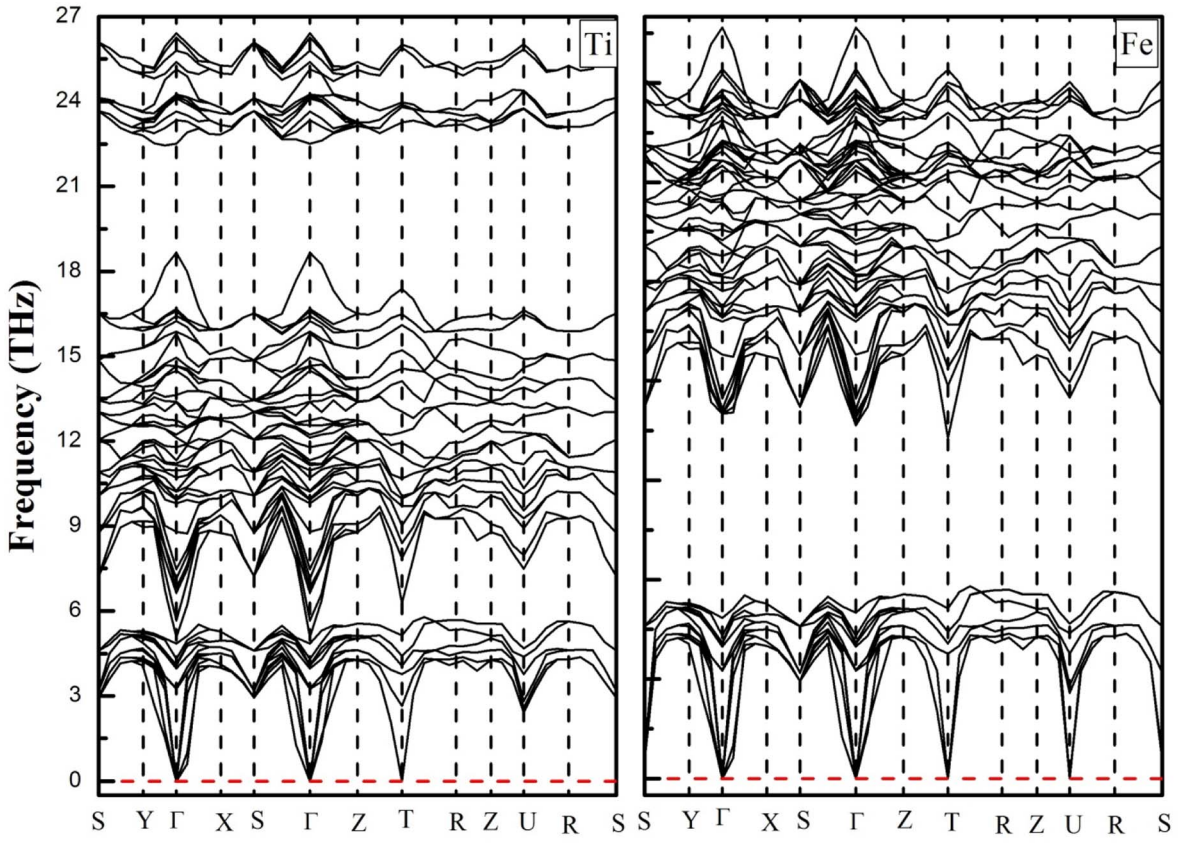

Fig. 3 Phonon dispersion curves of $YTiO_3$ and $YFeO_3$ compounds.

Open Access Article. Published on 31 January 2023. Downloaded on 12/12/2025 10:45:39 AM.
This article is licensed under a Creative Commons Attribution-NonCommercial 3.0 Unported Licence.

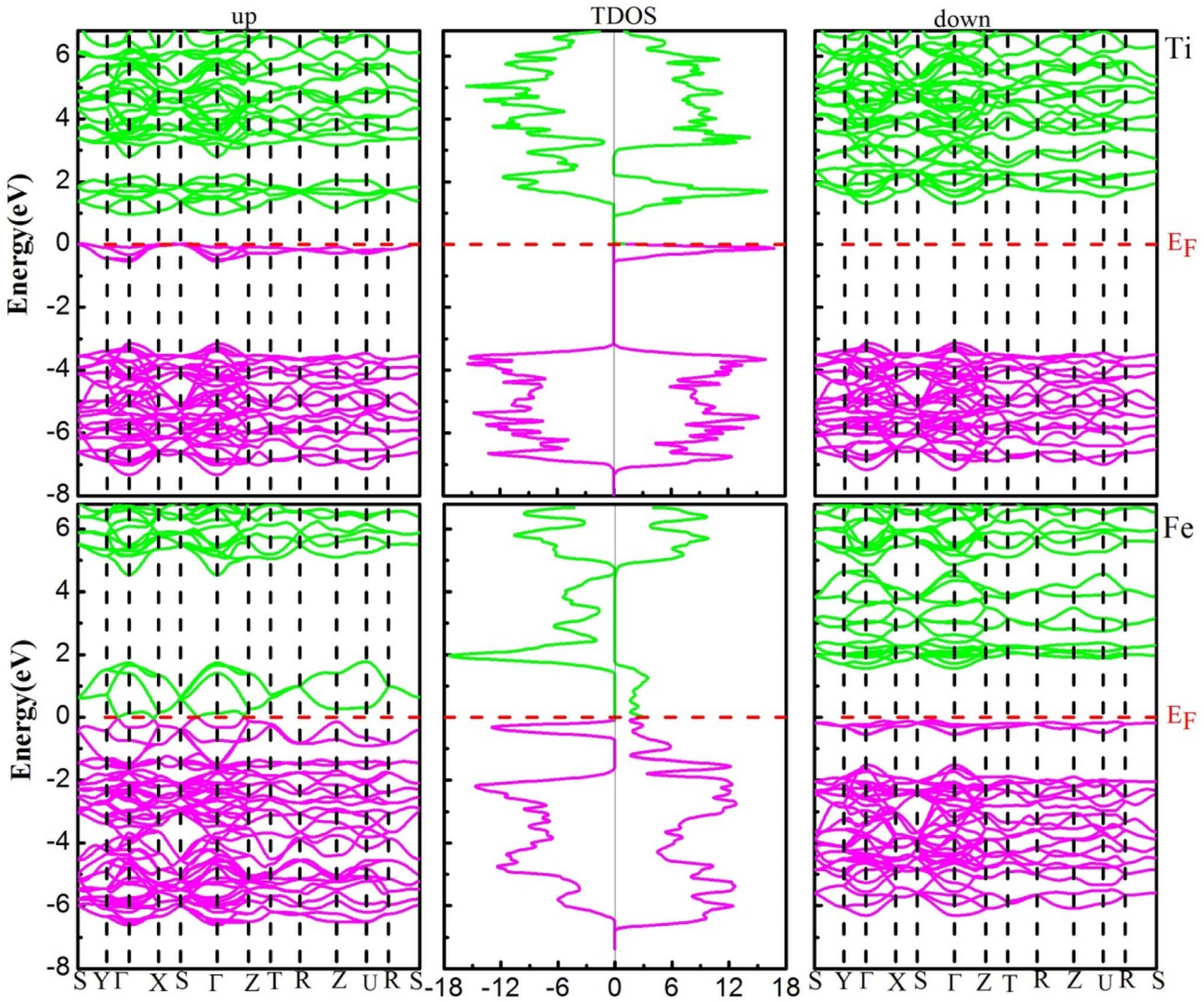

Fig. 4 The electronic band structure (left-up and right-down) and total density of states (middle) of YBO_3 perovskites. The Fermi level ($E_F = 0.0$ eV) is indicated by the horizontal dashed red line.

3.4. Mechanical properties

It is essential to study the mechanical properties of materials for the possibilities of their application in a particular technical field, where they are closely related to its elastic constants, which can provide us with information including the bonding character, the ductility, hardness, or brittleness of the materials. There are nine independent elastic constants, namely C_{11}, C_{22}, C_{33}, C_{44}, C_{55}, C_{66}, C_{12}, C_{13}, and C_{23} characterize the elastic properties of an orthorhombic system, where C_{11}, C_{22}, and C_{33} are associated with linear resistance to compression along the axes a, b, and c respectively and the others C_{44}, C_{55}, C_{66}, C_{12}, C_{13}, and C_{23} are related to the crystal shape. Pressure can affect the mechanical properties of a material such as hardness, stability, and even the phase structure of the material, and thus can limit its possibilities to use in industrial applications. In addition, for an orthodontic system to be mechanically stable, under pressure, it must meet the following criteria[18,44]

$$\tilde{C}_{ii} > 0;\ i = (1\text{–}6) \quad (2)$$

$$\tilde{C}_{11} + \tilde{C}_{22} + \tilde{C}_{33} + 2\tilde{C}_{12} + \tilde{C}_{13} + \tilde{C}_{23} > 0 \quad (3)$$

$$\tilde{C}_{11} + \tilde{C}_{22} - 2\tilde{C}_{12} > 0 \quad (4)$$

$$\tilde{C}_{11} + \tilde{C}_{33} - 2\tilde{C}_{13} > 0 \quad (5)$$

$$\tilde{C}_{22} + \tilde{C}_{33} - 2\tilde{C}_{23} > 0 \quad (6)$$

The elastic constants (C_{ij}) of the two compounds have been calculated under $P = 0$, 5, 10, and 15 GPa constant pressure and displayed in Table 3 and represented in Fig. 6. It is clear that all the mechanical stability requirements are met, thus both compounds investigated are stable mechanically up to 15 GPa pressures. Moreover, it is worth noting that all the ECs (elastic constants) of both compounds increase in a nonlinear way, and also, the C_{11}, C_{22} and C_{33} are always higher than the rest of the

© 2023 The Author(s). Published by the Royal Society of Chemistry

Open Access Article. Published on 31 January 2023. Downloaded on 12/12/2025 10:45:39 AM.
This article is licensed under a Creative Commons Attribution-NonCommercial 3.0 Unported Licence.

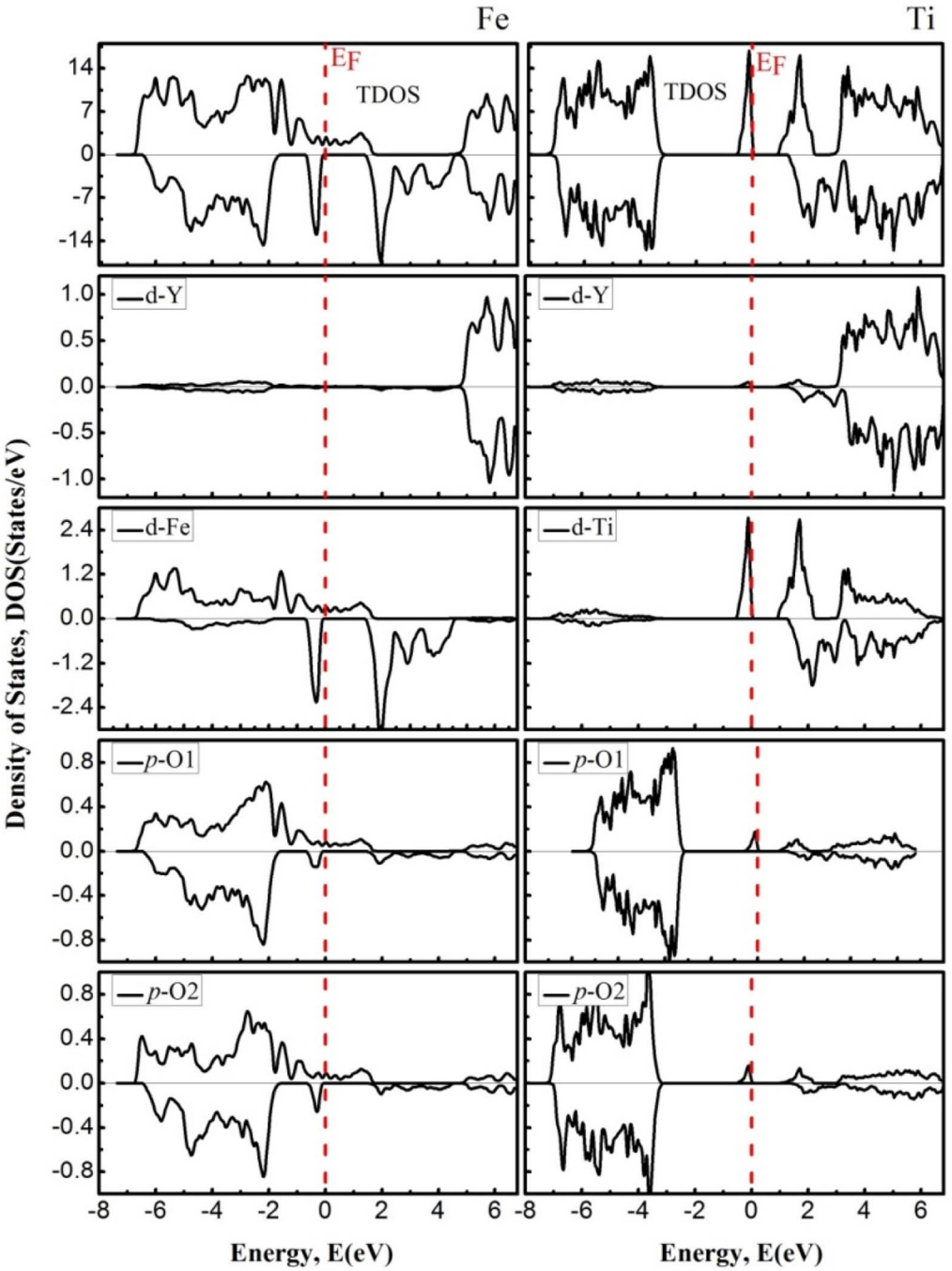

Fig. 5 The density of states of $YFeO_3$ perovskites (left) and $YTiO_3$ perovskites (right). The Fermi level (E_F = 0.0 eV) is indicated by the vertical dashed red line.

Table 2 The computed total and partial magnetic moments and the interstitial site in μ_B (Bohr magneton)

Compound	Total (μ_B)	Y (μ_B)	Fe/Ti (μ_B)	O (μ_B)	O (μ_B)	Interstitial (μ_B)
$YTiO_3$	4.00	0.01	0.73	0.00	0.00	0.92
$YFeO_3$	12.00	0.00	2.81	0.01	−0.01	0.69

other ECs, which means that the resistance to deformation along of the axial directions is stronger than that in the non-axial directions of the two compounds, in the pressure range studied.

Using the Voigt–Reuss–Hill approximation, some mechanical properties including Young's modulus E, bulk modulus B, shear modulus G, Pugh's coefficient G/B, Poisson's ratio ν, and Cauchy pressure C_P are calculated through the elastic constants. The details of these parameters are available in a recent paper.[18]

© 2023 The Author(s). Published by the Royal Society of Chemistry

Open Access Article. Published on 31 January 2023. Downloaded on 12/12/2025 10:45:39 AM.
This article is licensed under a Creative Commons Attribution-NonCommercial 3.0 Unported Licence.

Table 3 The evaluated elastic constants (C_{ij} in GPa)

	Pressure	C_{11}	C_{22}	C_{33}	C_{44}	C_{55}	C_{66}	C_{12}	C_{13}	C_{23}
$YTiO_3$	0	297	239	295	72	84	93	125	135	104
	5	360	319	353	107	127	123	131	137	113
	10	428	387	421	109	134	127	154	161	145
	15	430	384	426	124	150	141	147	159	129
$YFeO_3$	0	174	280	315	88	33	49	106	95	85
	0[a]	243[a]	169[a]	232[a]	113[a]	75[a]	78[a]	113[a]	99[a]	117[a]
	5	274	240	305	92	89	104	142	100	101
	10	323	285	349	97	109	118	145	129	110
	15	352	358	394	117	126	143	136	126	129

[a] Ref. 38.

The values of B, G, E, G/B, and ν computed for orthorhombic compounds $YTiO_3$ and $YFeO_3$ under pressure up to 15 GPa are presented in Table 4. Each of B, G, and E increases almost linearly for two compounds at different pressure, except for the 15 GPa, at which the bulk modulus of $YTiO_3$ loses little of its acquired value. Conversely, the Poisson's ratio "ν" decreases with increasing pressure. Moreover, for the entire range of pressure, the bulk modulus always exceeds the shear modulus, demonstrating the limiting factor for the mechanical stability of $YTiO_3$ and $YFeO_3$ compounds. Furthermore, the B and G values of the $YTiO_3$ remain higher than those of the $YFeO_3$, and thus the $YTiO_3$ has a greater ability to resist deformation compared

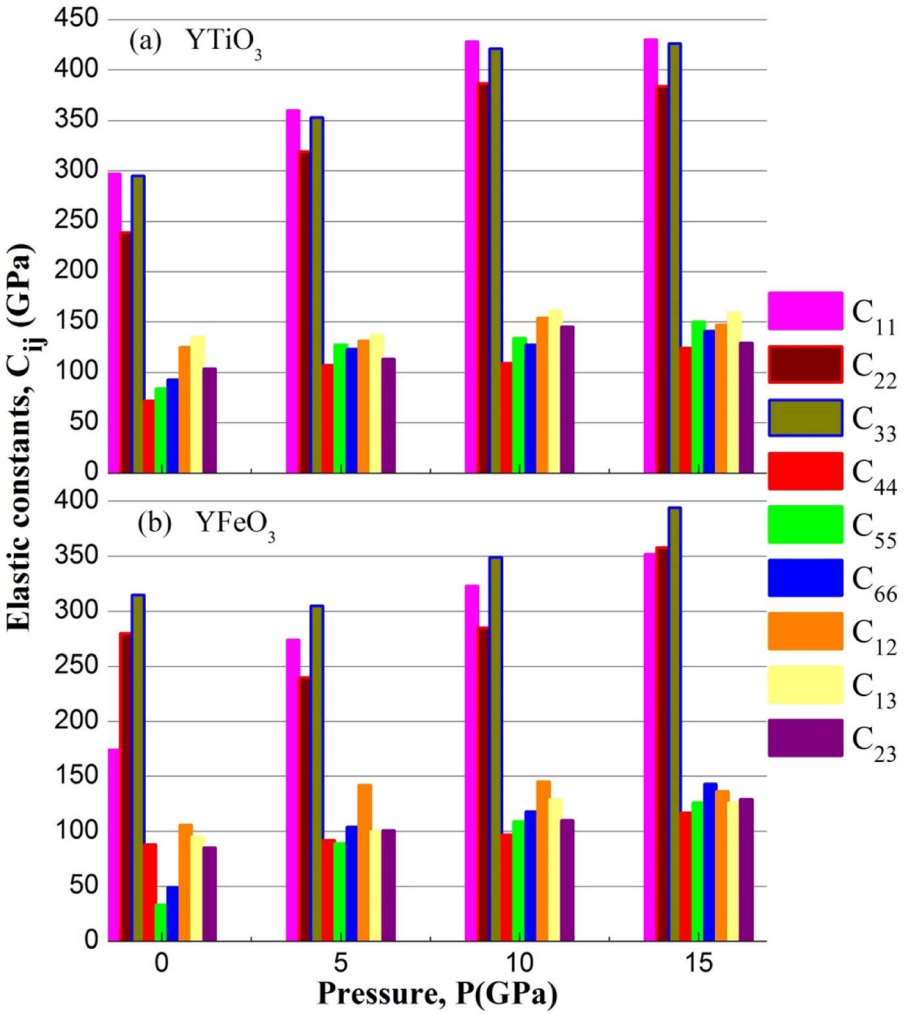

Fig. 6 The elastic constants of YBO_3 *versus* pressure.

© 2023 The Author(s). Published by the Royal Society of Chemistry

Open Access Article. Published on 31 January 2023. Downloaded on 12/12/2025 10:45:39 AM. This article is licensed under a Creative Commons Attribution-NonCommercial 3.0 Unported Licence.

Table 4 The elastic modulus (B, G, and E in GPa), Poisson's ratio (ν), Pugh ratio (G/B), and Vickers hardness (H_V in GPa) computed for orthorhombic oxides perovskite YBO_3 (B = Ti & Fe)

Compounds	Pressure	B	G	E	G/B	μ_M	ν	H_v
$YTiO_3$	0	172	80	209	0.46	2.38	0.29	7.60
	5	199	114	288	0.57	1.85	0.28	10.64
	10	239	125	320	0.53	2.19	0.27	12.78
	15	234	136	342	0.58	1.88	0.25	15.76
$YFeO_3$	0	145	61	160	0.42	1.64	0.31	5.04
	5	167	86	221	0.51	0.81	0.28	9.45
	10	191	102	260	0.53	1.96	0.27	11.36
	15	209	124	311	0.59	1.78	0.25	15.21

to the $YFeO_3$. Poisson's ratio "ν" is a significant parameter that provides us with some key properties of crystalline solids which are often utilized to infer the types of bonding. If the value of "ν" is less than 0.25, the character of the chemical bonding is covalent whereas, its value greater than 0.25 usually shows the ionic bonding character. The values of the Poisson's ratio computed for both the oxides perovskite materials are higher than 0.25, which indicates the ionic bonding character in the range of 0 GPa to 15 GPa pressure. The ductile or brittle nature of materials can be classified by G/B (Pugh's ratio) as well as by "ν" (Poisson's ratio), which is of great importance in determining the integrity of structures and industrial applications. According to Pugh, the critical value for separating brittle from ductile materials is G/B = 0.57. Brittle materials have a Pugh ratio higher than the critical value while ductile materials have a lower value than 0.57. Conversely, when the "ν" (Poisson's ratio) is higher than 0.26, the material shows ductility, and if the opposite, it becomes brittle. The values of the Pugh ratio (G/B) and the Poisson's ratio "ν" at 0 GPa pressure confirm that the two compounds studied are ductile materials. And with increasing pressure up to 15 GPa, the Pugh ratio values increase to reach 0.58 and 0.59 for $YTiO_3$ and $YFeO_3$ respectively, and conversely the values of Poisson's ratio decrease up to a value of 0.25 for both compounds, which means that both compounds tend to lose ductility with increasing pressure.

The "μ_M" is the machinability index that characterizes the cutting ability of a material, the maximum financial level of the plastic strain machine operation, and that is crucial for industrial zones[19] and is investigated using the following expression.

$$\mu_M = \frac{B}{C_{44}} \tag{7}$$

For both compounds, the calculated values of μ_M are displayed in Table 5, denoting enhanced lubricating characters and lesser frictions, which indicates the suitability of this material for industrial applications.

Hardness is a very important parameter in the world of mechanics which expresses the resistance of a material to corrosion. The most corrosion-resistant materials are the materials that have the highest hardness value. The Vickers hardness of a polycrystalline material can be calculated based on the bulk and shear moduli by following Chin's formula.[21,32]

Table 5 The evaluated A_1, A_2, and A_3 (shear anisotropic) parameters for the three different shear planes

Compounds	Pressure	A_1	A_2	A_3
$YTiO_3$	0	0.89	1.03	1.30
	5	0.97	1.13	1.17
	10	0.82	1.03	1.00
	15	0.92	1.08	1.08
$YFeO_3$	0	1.17	0.31	0.80
	5	0.97	1.03	1.80
	10	0.93	1.05	1.48
	15	0.94	1.02	1.30

$$H_v = 2\left(\frac{G^3}{B^2}\right)^{0.585} - 3 \tag{8}$$

The Vickers hardness results under increasing pressures up to 15 GPa are presented in Table 4, and it is worth noting that under the same pressure, $YTiO_3$ has a higher Vicker hardness value than $YFeO_3$, so it can be said that the $YTiO_3$ compound is harder than $YFeO_3$ compound, and the hardness of both compounds increases with increasing pressure within the pressure limits studied. The hardness of the studied compounds are similar to those of MAX phases, which are well-known damage-tolerant.[19] For the orthorhombic system, there are three shear anisotropic factors A_1, A_2, and A_3 (ref. 18 and 44) which are;

$$A_1 = \frac{4C_{44}}{C_{11} + C_{33} - 2C_{13}} \tag{9}$$

$$A_2 = \frac{4C_{55}}{C_{11} + C_{33} - 2C_{23}} \tag{10}$$

$$A_3 = \frac{4C_{66}}{C_{11} + C_{22} - 2C_{12}} \tag{11}$$

Whereas, the A_1 is along the {1 0 0} plane within the directions of [011] and [010]. The A_2 is along the {0 1 0} plane within the [101] and [001] directions and within the [110] and [010] directions the A_3 is along the {0 0 1} plane. As known, if the anisotropy factor A_i is equal to 1, then it reveals that the compound is completely isotopic, otherwise, it measures the degree of variability in the elasticity of the crystal. The calculations of the values of the shear anisotropic factors for $YTiO_3$ and $YFeO_3$ were performed under pressures of 0 to 15 GPa, and the results are in Table 5. All the values of the shear anisotropy factors deviate from "1", confirming that the $YTiO_3$ and $YFeO_3$ compounds are anisotropic materials in different directions and that this anisotropy remains present under the applied pressures.

3.5. Thermal properties

In the context of scientific and technological research, the determination of the thermal properties of materials plays an important role. Debye temperature (θ_D) is a significant parameter in determining the thermodynamic property of solid crystalline materials, as it relates to many physical properties,

Open Access Article. Published on 31 January 2023. Downloaded on 12/12/2025 10:45:39 AM. This article is licensed under a Creative Commons Attribution-NonCommercial 3.0 Unported Licence.

including the melting point, elastic constants, lattice thermal conductivity, and specific heat. According to Anderson, the value of Debye temperature θ_D can be deduced from the sound velocities *via* the below equations.[45,46]

$$\theta_D = \frac{h}{k_B}\left[\frac{3n}{4\pi}\left(\frac{N_A\rho}{M}\right)\right]^{1/3} \times v_m \quad (12)$$

$$v_m = \left[\frac{1}{3}\left(\frac{2}{{v_t}^3} + \frac{1}{{v_l}^3}\right)\right]^{-1/3} \quad (13)$$

$$v_l = \left(\frac{3B + 4G}{3\rho}\right)^{1/2} \quad (14)$$

$$v_t = \left(\frac{G}{\rho}\right)^{1/2} \quad (15)$$

where h is Plank's constant, n is the number of atoms in the unit cell, N_A represents Avogadro's number, ρ is the density, k_B depicts the Boltzmann's constant, M shows the molecular weight, v_l, v_m, and v_t is the longitudinal, average sound velocity, and transverse sound velocity respectively. Using the previously calculated results for the elastic constants, we have calculated the v_t, v_l, v_m and θ_D for each $YTiO_3$ and $YFeO_3$ compound under pressure up to 15 GPa, and the outcomes are listed in Table 6, and the evolutions of (θ_D) change with pressure are represented in the Fig. 7c. It is obvious that all sound velocities v_t, v_l, v_m, and Debye temperature are larger in $YTiO_3$ than in $YFeO_3$ at the same pressure, and all these values increase linearly with the increase in pressure. The high Debye temperature of both tested compounds makes them good candidates used in harsh environments.[47] Moreover, the T_m (melting temperature) is employed to know the purity of organic and inorganic materials. It also allows us to know the applicability of the material at high temperatures since solids can be used at temperatures below "T_m" unless oxidized by chemical change or excessive distortion causing mechanical/elastic failure. For both $YTiO_3$ and $YFeO_3$ compounds the T_m (melting temperature) is calculated using the following expression.[18,19,21,22,48]

$$T_m = 354(\mathrm{K}) + \frac{3}{2}\left(\frac{\mathrm{K}}{\mathrm{GPa}}\right)(2C_{11} + C_{33}) \quad (16)$$

The calculated melting point values at certain fixed pressures for the investigated compounds are presented in Table 5 and shown in Fig. 7d. It is worth noting that all the compounds have a high T_m with an advantage always in favor of $YTiO_3$ at the same pressure. T_m increases almost linearly for both compounds. Upon reaching 10 GPa, the intensity of the increase for $YTiO_3$ decreases. The general trend is that a higher melting temperature is associated with the higher elastic constants that indicate the strength of underlying bonding between atoms in a solid. These results confirm that these compounds are suitable in the thermally strict zone.

The lattice thermal conductivity is an essential property of solids. Here we have investigated the variation of the lattice thermal conductivity K_{ph} of our compounds with temperature using the Slack model:[49]

$$K_{ph} = A\frac{M_{av}{\theta_D}^3\delta}{\gamma^2 n^{2/3} T} \quad (17)$$

where M_{av} represents the average atomic mass of a crystal in kg mol^{-1}, δ defines the cubic root of average atomic volume in m, and γ mentions the Grüneisen constant and it can be calculated by the following formula;

$$\gamma = \frac{3(1+v)}{2(2-3v)} \quad (18)$$

where factor A is calculated as:

$$A = \frac{5.720 \times 10^7 \times 0.849}{2 \times \left(1 - \frac{0.514}{\gamma} + \frac{0.514}{\gamma^2}\right)} \quad (19)$$

Fig. 7a, b represents the variation of K_{ph} with temperature under a certain pressure of the $YTiO_3$ and $YFeO_3$. It is noted that the K_{ph} of $YTiO_3$ is mostly greater than that of $YFeO_3$ at the same pressure and temperature. The K_{ph} values gradually decrease with increasing temperature at certain constant pressures. Otherwise, at a constant temperature, the values of K_{ph} increase with increasing pressure almost linearly of the two compounds studied. Additionally, another important parameter is the minimum thermal conductivity κ_{min} which is defined as the theoretical minimum thermal conductivity at elevated

Table 6 Investigated density (ρ in g cm^{-3}), longitudinal, transverse, and average elastic wave velocities (v_t, v_l, v_m in m s^{-1}), Debye temperature (θ_D in K), Melting temperature (T_m in K), minimum thermal conductivity and lattice thermal conductivities (k_{min}, k_{ph} in W m^{-1} K^{-1})

Compounds	Pressure	ρ (g cm^{-3})	v_l	v_t	v_m	θ_D	T_m	k_{min}	k_{ph}
$YTiO_3$	0	5.23	7312	3928	4386	574	1687	0.40	53.44
	5	5.35	8108	4629	5144	679	1963	0.47	72.83
	10	5.47	8623	4789	5334	709	2269	0.50	116.02
	15	5.58	8645	4945	5494	735	2283	0.52	148.27
$YFeO_3$	0	5.67	6324	3278	3669	487	1348	0.34	29.00
	0[a]	…	…	…	3381[a]	449[a]	…	…	…
	5	5.84	6958	3850	4290	575	1633	0.41	62.18
	10	6.00	7390	4126	4594	621	1846	0.44	81.72
	15	6.15	7813	4495	4992	680	2001	0.49	123.65

[a] Ref. 38.

© 2023 The Author(s). Published by the Royal Society of Chemistry

Open Access Article. Published on 31 January 2023. Downloaded on 12/12/2025 10:45:39 AM.
This article is licensed under a Creative Commons Attribution-NonCommercial 3.0 Unported Licence.

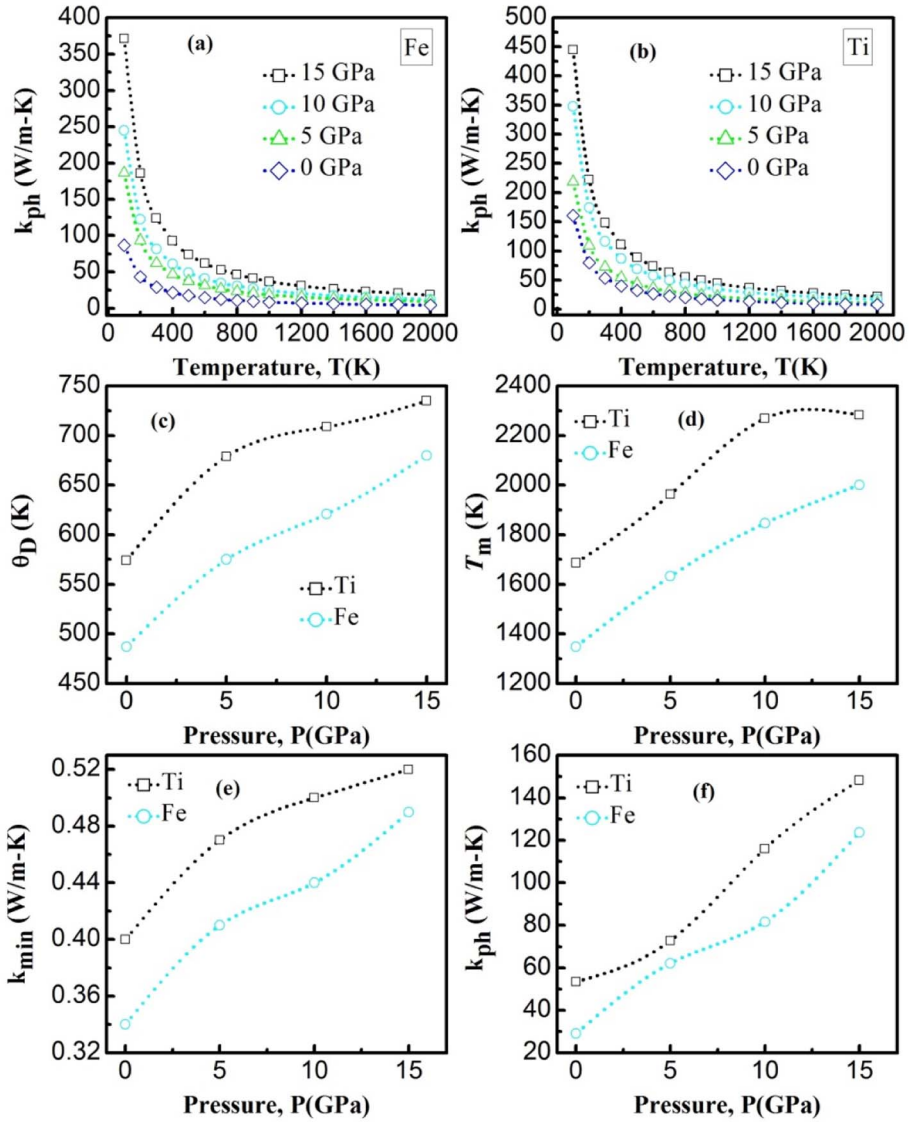

Fig. 7 The (a) and (b) is the temperature dependence of the lattice thermal conductivity of YBO_3. The (c) and (d) is the Debye temperature and melting temperature for YBO_3 as a function of different pressure. The (e) and (f) is the minimum and lattice thermal conductivity for YBO_3 as a function of different pressure.

temperatures with Debye temperatures and was estimated using the Clarke model given by the following expression.[50,51]

$$\kappa_{\min} = 0.87k_B\left(\frac{M}{n\rho N_A}\right)^{-2/3}\sqrt{\frac{E}{\rho}} \quad (20)$$

Fig. 7e plotted the variation of κ_{min} with the pressure of the $YTiO_3$ and $YFeO_3$. From Fig. 7e, it is observed that κ_{min} rises with the increase in pressure of both compounds, and like all time $YTiO_3$ has higher values than $YFeO_3$ at the same pressure. It is recognized that an optimum limit of κ_{min} <1.25 W mK^{-1} is suitable for TBC materials.[52] Therefore, we can say that both compounds demonstrates can be an optimum material for TBC applications.

4. Conclusion

In this work, the WIEN2K simulation code is utilized for investigating several physical properties comprising the structural, mechanical, thermal, magnetic, and electronic properties of orthorhombic oxides perovskite YBO_3 (B = Ti & Fe) through the FP-LAPW incorporated within the WIEN2K. The YBO_3 is recognized to be a potential half-metallic ferromagnetic material. The computed formation energy signifies the thermodynamic and structural stability of the investigated compounds. The ductility and mechanical stability of both materials are confirmed from the investigations of elastic properties and these compounds possess ionic bonding character dominantly. The values for thermal parameters (high melting temperature and low minimum thermal conductivity) for these compounds

© 2023 The Author(s). Published by the Royal Society of Chemistry

Open Access Article. Published on 31 January 2023. Downloaded on 12/12/2025 10:45:39 AM. This article is licensed under a Creative Commons Attribution-NonCommercial 3.0 Unported Licence.

were estimated as a promising material for TBC and hostile environments applications. These results demonstrate the possibility of using YBO_3 materials in modern technology and mechanical applications.

Conflicts of interest

There are no conflict to declare.

Acknowledgements

The authors extend their appreciation to the Deanship of Scientific Research at King Khalid University for funding this work support through the research groups program under grant number (RGP.2/145/43). The authors are also thankful to the Taif University Researchers Supporting Project number (TURSP-2020/03), Taif University, Taif, Saudi Arabia.

References

1 A. Azzouz-Rached, M. A. Hadi, H. Rached, T. Hadji, D. Rached and A. Bouhemadou, *J. Alloys Compd.*, 2021, **885**, 160998, DOI: 10.1016/j.jallcom.2021.160998.
2 M. Mehl, J. Osburn, D. Papaconstantopoulos and B. Klein, *Phys. Rev. B*, 1990, **41**, 10311, DOI: 10.1103/PhysRevB.41.10311.
3 N. P. Padture, *Nat. Mater.*, 2016, **15**, 804–809, DOI: 10.1038/nmat4687.
4 W. Pan, S. R. Phillpot, C. L. Wan and et al, ., *MRS Bull.*, 2012, **37**, 917–922, DOI: 10.1557/mrs.2012.234.
5 J. Y. Yuan, J. B. Sun, J. S. Wang and et al, ., *J. Alloys Compd.*, 2018, **740**, 519–528, DOI: 10.1016/j.jallcom.2018.01.021.
6 Y. C. Liu, V. R. Cooper, B. H. Wang and et al, ., *Mater. Res. Lett.*, 2019, **7**, 145–151, DOI: 10.1080/21663831.2019.1566183.
7 Y. Liu, K. Chu, Y. Zhou, Y. Li, W. Li and B. Liu, *J. Adv. Ceram.*, 2022, **11**, 1596–1603, DOI: 10.1007/s40145-022-0632-0.
8 X. J. Wang, Y. Huan, Y. X. Zhu and et al, ., *J. Adv. Ceram.*, 2022, **11**, 184–195, DOI: 10.1007/s40145-021-0526-6.
9 A. A. Adeleke, S. A. Bonev, C. J. Wu, E. E. Jossou, and E. R. Johnson. arXiv preprint arXiv, 2022, 2209-05652. DOI: 10.48550/arXiv.2209.05652.
10 A. A. Adeleke, A. O. Adeniyi, H. Tang, H. Gou and Y. Yao, *J. Phys.: Condens. Matter*, 2020, **32**, 395401, DOI: 10.1088/1361-648X/ab96f1.
11 A. A. Adeleke and Y. Yao, *Phys. Chem. Chem. Phys.*, 2019, **21**, 7508–7517, DOI: 10.1039/C8CP07288D.
12 A. Majumdar, A. A. Adeleke, S. Chakraborty and R. Ahuja, *J. Mater. Chem. C*, 2020, **8**, 16392–16403, DOI: 10.1039/D0TC04516K.
13 A. A. Adeleke, E. E. Jossou, N. U. Ukoji, A. O. Adeniyi and P. O. Egbele, *ACS Omega*, 2020, **5**, 26786–26794, DOI: 10.1021/acsomega.0c03880.
14 Y. Wang, Z. Lv, L. Zhou, X. Chen, J. Chen, Y. Zhou and S. T. Han, *J. Mater. Chem. C*, 2018, **6**, 1600–1617, DOI: 10.1039/C7TC05326F.
15 M. Johnsson and P. Lemmens, *J. Phys.: Condens. Matter*, 2008, **20**, 264001, DOI: 10.1088/0953-8984/20/26/264001.
16 G. Pilania, P. V. Balachandran, C. Kim and T. Lookman, *Front. Mater.*, 2016, **3**, 19, DOI: 10.3389/fmats.2016.00019.
17 I. Petousis, Density functional theory and machine learning methods for dielectric materials discovery, Doctoral dissertation, Stanford University, 2016.
18 W. Hasan, A. M. Hossain, M. Rasheduzzaman, M. A. Rahman, M. M. Hossain, K. R. Mohammad and M. Z. Hasan, *RSC Adv.*, 2022, **12**, 27492–27507, DOI: 10.1039/D2RA04273H.
19 M. A. Hadi, M. N. Islam and M. H. Babu, *Z. Naturforsch., A: Phys. Sci.*, 2019, **74**, 71–81, DOI: 10.1515/zna-2018-0334.
20 A. Azzouz-Rached, M. W. Qureshi, I. Ouadha, H. Rached, T. Hadji and H. Rekab-Djabri, *Comput. Condens. Matter*, 2022, **33**, e00748, DOI: 10.1016/j.cocom.2022.e00748.
21 A. Azzouz-Rached, Md. M. H. Babu, H. Rached, T. Hadji and D. Rached, *Mater. Today Commun.*, 2021, **27**, 102233, DOI: 10.1016/j.mtcomm.2021.102233.
22 A. Azzouz-Rached, H. Rached, M. H. Babu, T. Hadji and D. Rached, *Int. J. Quantum Chem.*, 2021, **121**, e26770, DOI: 10.1002/qua.26770.
23 P. Hohenberg and W. Kohn, *Phys. Rev.*, 1964, **136**, B864, DOI: 10.1103/PhysRev.136.B864.
24 P. Blaha, K. Schwarz, F. Tran, R. Laskowski, G. K. H. Madsen and L. D. Marks, *J. Chem. Phys.*, 2020, **152**, 074101, DOI: 10.1063/1.5143061.
25 T. Hadji, H. Khalfoun, H. Rached, Y. Guermit, A. Azzouz-Rached and D. Rached, *Eur. Phys. J. B*, 2020, **93**, 214, DOI: 10.1140/epjb/e2020-10204-5.
26 J. P. Perdew, K. Burke and M. Ernzerhof, *Phys. Rev. Lett.*, 1996, **77**, 3865.
27 J. P. Perdew, K. Burke and M. Ernzerhof, *Phys. Rev. Lett.*, 1997, **78**, 1396.
28 V. I. Anisimov and O. Gunnarsson, *Phys. Rev. B*, 1991, **43**, 7570, DOI: 10.1103/PhysRevB.43.7570.
29 V. I. Anisimov, J. Zaanen and O. K. Andersen, *Phys. Rev. B*, 1991, **44**, 943, DOI: 10.1103/PhysRevB.44.943.
30 V. I. Anisimov, I. V. Solovyev, M. A. Korotin, M. T. Czyżyk and G. A. Sawatzky, *Phys. Rev. B*, 1993, **48**, 16929, DOI: 10.1103/PhysRevB.48.16929.
31 I. Khan, I. Ahmad, I. U. Haq, A. Ali, Z. Ali and I. Ahmad, *J. Electron. Mater.*, 2020, **49**, 3357–3366, DOI: 10.1007/s11664-020-08048-3.
32 H. Rached, S. Bendaoudia and D. Rached, *Mater. Chem. Phys.*, 2017, **193**, 453–469, DOI: 10.1016/j.matchemphys.2017.03.006.
33 A. Ali, I. Khan, Z. Ali, F. Khan and I. Ahmad, *Int. J. Mod. Phys. B*, 2019, **33**, 1950231, DOI: 10.1142/S021797921950231X.
34 H. C. Kandpal, G. H. Fecher, C. Felser and G. Schönhense, *Phys. Rev. B*, 2006, **73**, 094422, DOI: 10.1103/PhysRevB.73.094422.
35 B. Balke, G. H. Fecher, H. C. Kandpal, C. Felser, K. Kobayashi, E. Ikenaga and S. Ueda, *Phys. Rev. B*, 2006, **74**, 104405, DOI: 10.1103/PhysRevB.74.104405.

© 2023 The Author(s). Published by the Royal Society of Chemistry

Open Access Article. Published on 31 January 2023. Downloaded on 12/12/2025 10:45:39 AM.
This article is licensed under a Creative Commons Attribution-NonCommercial 3.0 Unported Licence.

36 I. Khan, I. Ahmad, I. U. Haq, A. Ali, Z. Ali and I. Ahmad, *J. Electron. Mater.*, 2020, **49**, 3357–3366, DOI: **10.1007/s11664-020-08048-3**.
37 L. Suthar, V. K. Jha, F. Bhadala, M. Roy, S. Sahu and S. K. Barbar, *Appl. Phys. A*, 2017, **123**, 1–9, DOI: **10.1007/s00339-017-1272-z**.
38 M. Romero, R. Escamilla, V. Marquina and R. Gómez, *Eur. Phys. J. D*, 2015, **69**, 1–6, DOI: **10.1140/epjd/e2015-60186-4**.
39 I. Ouadha, H. Rached, A. Azzouz-Rached, A. Reggad and D. Rached, *Comput. Condens. Matter*, 2020, **23**, e00468, DOI: **10.1016/j.cocom.2020.e00468**.
40 A. Azzouz-Rached, H. Rached, I. Ouadha, D. Rached and A. Reggad, *Mater. Chem. Phys.*, 2021, **260**, 124189, DOI: **10.1016/j.matchemphys.2020.124189**.
41 T. Hadji, H. Khalfoun, H. Rached and A. Azzouz-Rached, *Mater. Res. Bull.*, 2021, **143**, 111461, DOI: **10.1016/j.materresbull.2021.111461**.
42 T. Hadji, H. Khalfoun, H. Rached and A. Azzouz-Rached, *Comput. Condens. Matter*, 2021, **27**, e00557, DOI: **10.1016/j.cocom.2021.e00557**.
43 K. Bendriss, H. Rached, I. Ouadha and et al, ., *Indian J. Phys.*, 2022, 1–11, DOI: **10.1007/s12648-022-02482-1**.
44 D. Segall, P. J. D. Lindan, M. J. Probert, C. J. Pickard, P. J. Hasnip, S. J. Clark and M. C. Payne, *J. Phys.: Condens. Matter*, 2002, **14**, 2717–2744, DOI: **10.1088/0953-8984/14/11/301**.
45 T. Rackl, L. Eisenburger, R. Niklaus and D. Johrendt, *Phys. Rev. Mater.*, 2019, **3**, 054001, DOI: **10.1103/PhysRevMaterials.3.054001**.
46 O. L. Anderson, *J. Phys. Chem. Solids*, 1963, **24**, 909–917, DOI: **10.1016/0022-3697(63)90067-2**.
47 D. R. Clarke and S. R. Phillpot, *Mater. Today*, 2005, **8**, 22–29, DOI: **10.1016/S1369-7021(05)70934-2**.
48 M. E. Fine, L. D. Brown and H. L. Mercus, *Scr. Metall.*, 1984, **18**, 951–956, DOI: **10.1016/0036-9748(84)90267-9**.
49 D. T. Morelli and G. A. Slack, *High Thermal Conductivity Materials*, ed. S. L. Shindé and J. S. Goela, Springer, New York, 2006. DOI: **10.1007/b106785**.
50 D. R. Clarke, *Surf. Coat. Technol.*, 2003, **163–164**, 67–74, DOI: **10.1016/S0257-8972(02)00593-5**.
51 Y. Liu, V. R. Cooper, B. Wang, H. Xiang, L. Qian, Y. Gao, J. Yang, Y. Zhou and B. Liu, *Mater. Res. Lett.*, 2019, **7**, 145–151, DOI: **10.1080/21663831.2019.1566183**.
52 Y. Liu, V. R. Cooper, B. Wang, H. Xiang, L. Qian, Y. Gao, J. Yang, Y. Zhou and B. Liu, *Mater. Res. Lett.*, 2019, **7**, 145–151, DOI: **10.1080/21663831.2019.1566183**.

© 2023 The Author(s). Published by the Royal Society of Chemistry